Excess Carriers Induced in Indium Antimonide with a Carbon-Dioxide Laser*

H. J. Fossum,†‡ W. S. Chen, and B. Ancker-Johnson§
Boeing Aerospace Company, Seattle, Washington 98124
and University of Washington, Seattle, Washington 98195
(Received 27 March 1973)

Production of high excess-carrier densities, i.e., plasmas, in n-InSb irradiated with CO_2-laser light is accomplished by two-photon excitation of electron-hole pairs. The properties of such plasmas are found by photoconductivity, infrared-absorption, and recombination-radiation measurements, at liquid-N_2 and -He temperatures, with both 10.6- and 9.6-μm irradiation wavelengths. Maximum excess-carrier densities obtained are $\approx 10^{15}$ cm^{-3} at 77 °K and $\approx 5 \times 10^{15}$ cm^{-3} at 4 °K. In samples with thickness ≤ 0.3 mm, uniform carrier distributions are obtained throughout the bulk of the samples. This feature plus the absence of applied electric fields during the plasma-generation process make these plasmas unique. In samples with thicknesses ≥ 0.3 mm, free-hole absorption of the CO_2-laser radiation causes the plasma density to be reduced in the far end of the sample. Absorption measurements yield a value for the free-hole-absorption cross section, $q \approx 5 \times 10^{-15}$ cm^2, which is in good agreement with the cross section measured for equilibrium holes by Kurnick and Powell. Shaping of the laser pulse during passage through the sample is observed and attributed to free-hole absorption which depends nonlinearly on the laser intensity.

I. INTRODUCTION

High excess-carrier densities have been produced in InSb single crystals by irradiation with CO_2-laser light of up to ~ 5-MW/cm^2 intensity in a temperature range of (4–300) °K.[1–4] The excess-carrier densities, i.e., plasmas, result from two-photon excitation of electron-hole pairs, a mechanism that is well understood.[5] In this paper two-photon-generated plasmas are studies systematically by means of excess-conductivity, infrared-absorption, and recombination-radiation measurements for irradiation intensities of up to ~ 15 MW/cm^2 at liquid-He and -N_2 temperatures. The results are compared with previous results if available.

A description of the experimental method in Sec. II is followed by the results of photoconductivity measurements in Sec. III A. Photoconductivity measurements have also been reported by Danishevskii *et al.* at liquid-N_2 temperature,[2] and by Slusher *et al.* at both liquid-N_2 and -He temperatures.[3] Our results differ somewhat from the ones obtained by Danishevskii *et al.* at 80 °K. They obtained a quadratic dependence between the excess conductivity of the sample and the irradiation intensity until, at high intensities, a saturation in the average excess conductivity occurs because of free-hole absorption. We obtain essentially the same conductivity characteristic except at the high irradiation intensities. At high intensities we find that the average excess conductivity changes to a linear dependence on the irradiation intensity. At the highest intensities both theirs and our results exhibit saturation caused by free-hole absorption. Slusher *et al.* report photoconductivity data for only one particular value of the incident laser irradiation since they concentrate on measuring plasma density by another technique, namely, by using a 17-μm laser beam as a density probe. Thus, only photoconductivity data of Danishevskii *et al.* are compared with our results.

The saturation attributed above to free-hole absorption is caused by a single-photon transition between the two valence bands. This effect is large compared to the absorption caused by the two-photon excitation. Some results of free-hole absorption are presented in Sec. III B, including a previously unreported shaping of the laser pulse when it passes through the InSb samples.

Recombination-radiation measurements are treated in Sec. III C. Recombination radiation is also reported by Slusher *et al.*; however, no measurements of the relation between the intensity of the recombination radiation and the CO_2-laser irradiation intensity are given with which to compare our results. At liquid-He temperatures we confirm the result obtained by Slusher *et al.*, that the duration of the recombination-radiation pulse is no longer than the laser pulse, except at the highest irradiation intensities when the sample is at least 0.5 mm thick.

The theory of radiative recombination and the comparison between theory and the results found in Sec. III C are reported elsewhere.[6,7]

II. EXPERIMENTAL METHOD

A. Experimental Arrangement

Figure 1 shows a block diagram of the experimental arrangement. A Q-switched CO_2 laser is used to illuminate n-type InSb samples and thereby

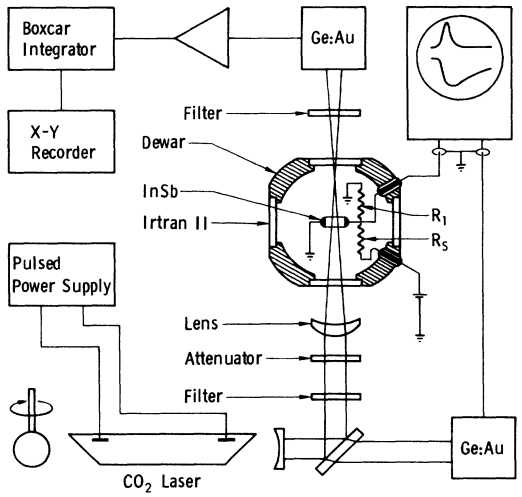

FIG. 1. Experimental arrangement. The lens is shifted away from the Dewar to increase the beam diameter impinging on the sample.

generate excess carriers in them. The laser is excited by a pulsed power supply and is adjustable to either 9.6- or 10.6-μm radiation wavelength. When the 9.6-μm wavelength is desired, a 9.6-μm dielectric bandpass filter is used inside the laser cavity. Alternatively, to ensure obtaining exclusively 10.6-μm radiation, a 10.6-μm dielectric bandpass filter is placed between the laser and the sample.

To regulate the radiation intensity impinging on the sample, two ways of attenuating the laser beam are available: sets of mounted Teflon sheets whose attenuation we calibrate, or a SF_6 gas cell with variable gas pressure.[8] When radiation densities higher than available with the unfocused laser beam are needed, a germanium lens with a 5-in. focal length is used to focus the beam.

The peak-power density in the center of the beam g_{max}, is determined from measurements of the average total power, the time dependence of the laser, and the intensity distribution over the cross section of the beam. A fraction of the laser beam passes through a partially reflecting mirror and is monitored by a gold-doped-germanium detector cooled to 77 °K. With this Ge : Au detector the time dependence and the power distribution over the cross section of the laser beam are measured. In the present experimental setup g_{max} is determined within a factor of 1.5; inaccuracy in the average power measurement is the source of almost all this error.

Another Ge : Au detector, also cooled to 77 °K, is used to measure the light passing through the sample or to measure the 5.3-μm recombination radiation from the sample. When it is used to detect the 5.3-μm radiation, a 5.3-μm bandpass filter is placed in front of this detector to filter out the radiation from the laser, as also shown in Fig. 1. The signal from the detector, in this case, is amplified with a low-noise amplifier, integrated by a boxcar integrator, and recorded. The boxcar integrator has a minimum aperture time of 10 μsec (maximum resolution).

The sample is kept in a variable-temperature Dewar with optical access through Irtran-II windows. The samples are immersed in either liquid N_2 or liquid He. In the latter case, to eliminate He boiling and the consequent laser-beam scattering, the temperature is reduced below the λ point.

The conductivity of each sample is measured by monitoring the voltage across it in the simple circuit included in Fig. 1. Terminated 50-Ω cables are used for all the signal paths. Since the inner and outer connector of our cryogenic coaxial cables are made of different material, the Seebeck effect (thermocouple voltage) causes a dc offset in the signal. This dc offset is balanced out in the oscilloscope.

Inspection of the circuit shows that we have the following relation between the measured voltage U and the excess conductivity σ_{ex}:

$$\sigma_{ex} = (l/A)\,G[(U_0/U) - 1]\,. \tag{1}$$

Here G is the sum $(1/R_1) + (1/R_S)$ + (the equilibrium conductance of the sample) + (the conductive load of the terminated coaxial cable). The resistors R_1 and R_S are shown in Fig. 1, l and A are the length (distance between contacts) and the cross section of the sample, respectively, and U_0 is the equilibrium voltage drop across the sample.

B. Properties of InSb Samples

The experiments reported in the present paper utilize exclusively n-type crystals because more nearly Ohmic contacts can be made on n-type InSb than on p type, for a large range of excess-carrier densities. This is explained and verified experimentally in Appendix A.

To make Ohmic contacts, indium containing 1-wt.% tellurium is alloyed onto polished n-InSb using Divco No. 300 rosen flux. The current-voltage characteristics of the resulting samples at 77 °K show Ohmic behavior for the entire range of excess-carrier densities obtained. When the samples are cooled down to liquid-He temperatures, however, the relation between current and voltage for samples with no excess carriers becomes linear only when the applied voltage exceeds 10 to 20 mV across the ~ 1-mm-long samples. This current-voltage characteristic agrees qualitatively with earlier measurements and is ascribed to the hot-electron effect.[9] (See Appendix B).

The non-Ohmic behavior at liquid-He temperatures causes σ_{ex} to be dependent on the voltage

across the sample. We cannot use a constant-voltage circuit to minimize this source of inaccuracy, since the samples when illuminated have a resistance that is only a fraction of an ohm. Hence, it is difficult to assign well-defined error brackets to the measured value of σ_{ex} at liquid-He temperatures (see Appendix B).

The physical properties of the n-InSb samples used are listed in Table I. The equilibrium conductivity σ_0 is measured individually for each sample. However, since the samples are too small to apply extra contacts for Hall measurements, we use the average electron mobility μ of the boule from which the sample is cut. The average electron mobility for all three boules is $\sim 7\times10^5$ cm^2/V sec at 77 °K and is estimated to be $\sim 10^5$ cm^2/V sec at 2 °K and 4 °K.[10]

III. RESULTS AND DISCUSSION

A. Excess-Conductivity Measurements

The excess conductivity of the samples is measured as a function of the CO_2-laser irradiation density at both liquid-N_2 and liquid-He temperatures. Since the half-power diameter of the laser beam is 2.2 mm, which is larger than the size of the samples by a factor of ~ 2, it is reasonable to assume that the illumination of the samples is uniform over the entire cross section. For the excess-carrier densities generated for these conductivity measurements, the attenuation of the laser light in the bulk of the samples is negligible. The attenuation of the laser beam during its passage through the sample that occurs when higher excess-carrier densities are generated is discussed in Sec. III B.

The generation and recombination of excess carriers are described by the following rate equation valid for any location within the sample if the surface recombination of excess carriers and loss of carriers through the contacts are negligible:

$$\frac{\partial n}{\partial t} = K_1 \mathcal{I} + K_2 \mathcal{I}^2 - \frac{n}{\tau} - r n(n+n_0). \qquad (2)$$

TABLE I. Physical properties of samples.

Boule no.	Sample no.	Size [mm]	σ_0(77 °K) [mho/cm]
W1017D	5*n*	1.05×1.00×0.35	No contacts
W1017D	9*n*	1.05×1.00×0.35	2.5
W1017D	12*n*	1.00×1.05×0.50	4.5
W1017D	13*n*	1.00×0.95×0.70	6.4
W1017D	17*n*	0.95×1.00×0.30	0.8
W508H	1*n*	1.00×1.00×0.33	6.2
W508H	2*n*	1.00×1.00×0.63	6.1
W508H	3*n*	1.00×0.99×1.16	5.8
W508H	4*n*	1.45×1.52×0.50	10.7

The first term accounts for single-photon excitations from levels in the middle of the band gap; the other generation term $K_2\mathcal{I}^2$ is caused by band-to-band two-photon excitation. In Eq. (2), n and n_0 are the excess and the equilibrium carrier densities, respectively, and $\mathcal{I}$ is the laser intensity. Both n and $\mathcal{I}$ are dependent on the time t. The nonradiative lifetime is represented by τ and the bimolecular recombination constant by r.

Equation (2) differs from the rate equation used by Slusher *et al.*,[3] in that we include the terms $K_1\mathcal{I}$, $-n/\tau$, and $-rnn_0$. The linear excitation term $K_1\mathcal{I}$ is important for laser intensities $\lesssim 1$ kW/cm^2, and experimentally we find that the monomolecular recombination described by the term n/τ dominates the radiative loss term rn^2 at 77 °K. Slusher *et al.* neglect n_0 in the radiative-recombination term, since they only consider the case $n \gg n_0$.

The single-photon generation described by the coefficient K_1 is caused by excitations from levels located between the valence and the conduction bands. K_1 is generally a function of the occupation probability of these levels. The two-photon generation coefficient K_2 is obtained from the measurements described in this section; K_2 is discussed in more detail and compared with theoretical values elsewhere.[5]

Since there are considerable differences between the results obtained at 77 °K and 2 °K, the measurements at these two temperatures will be discussed separately below. The main differences are caused by (i) $n/\tau \gg rn(n+n_0)$ for the entire range of n at 77 °K, while $n/\tau \ll rn(n+n_0)$ at 2 °K[6]; and (ii) K_2 vanishes at 2 °K for 10.6-μm laser wavelength, since the band-gap energy at 2 °K is sufficiently large so that the 10.6-μm laser irradiation is below the cutoff for the two-photon band-to-band transition.[5]

*a. At liquid-*He *temperatures.* Figure 2 shows the maximum value of the excess conductivity, $\sigma_{ex,max}$, as a function of the peak laser intensity, $\mathcal{I}_{max}$, at 2 °K for sample *W1017D-17n*. The half-power full width of the laser pulse, Δt, is given for each curve. For the range of $\mathcal{I}_{max}$ obtained, $\sigma_{ex,max}$ is proportional to $\mathcal{I}_{max}$ for both low and high values of $\mathcal{I}_{max}$ when the sample is exposed to 9.6-μm irradiation. We refer to these two linear regions as the low- and high-intensity regions, respectively. For intermediate values of $\mathcal{I}_{max}$ the slopes in the log-log plot reach a value as high as 2. The curves obtained with 10.6-μm irradiation differ from this description and will be discussed at the end of this subsection.

Next the experimental results obtained with 9.6-μm irradiation are fitted to Eq. (2). As mentioned above $n/\tau \ll rn(n+n_0)$ at 2 °K for all values of n, therefore, the term n/τ can be deleted from Eq. (2). In the low- and intermediate-intensity

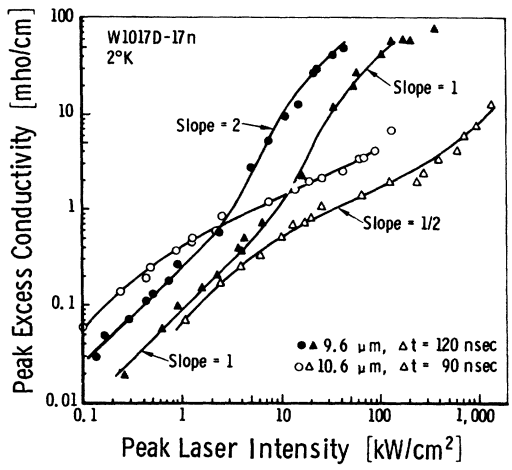

FIG. 2. Peak value of excess conductivity as a function of peak incident laser intensity. A focused beam (triangles) requires a higher $\mathcal{S}_{max}$ to obtain the same $\sigma_{ex,max}$ than an unfocused beam (circles) because the focused beam illuminates the sample somewhat nonuniformly.

regions the lifetime $[r(n+n_0)]^{-1}$ is much longer than Δt, thus, since the maximum value of σ_{ex} is obtained during the duration of the laser pulse, the last term does not contribute to $\sigma_{ex,max}$ and can also be neglected. The result of integrating the remaining two terms in Eq. (2) is, assuming that the laser has a gaussian time dependence,

$$\sigma_{ex,max} = e\mu n_{max} \approx 1.06 e\mu \Delta t K_1 (1-R)\, \mathcal{S}_{max} + 0.75 e\mu \Delta t K_2 (1-R)^2 (\mathcal{S}_{max})^2 . \quad (3)$$

Equation (3) shows that $\sigma_{ex,max}$ is proportional to $\mathcal{S}_{max}$ for low values of $\mathcal{S}_{max}$ and proportional to $(\mathcal{S}_{max})^2$ for higher (intermediate as defined above) values of $\mathcal{S}_{max}$, in agreement with the measurements. Curve fitting then yields $K_1 = 2\times 10^{10}$ $\text{erg}^{-1}\text{sec}^{-1}$ and $K_2 = 0.9$ cm sec/erg^2 for $\lambda = 9.6$ μm. (See Ref. 5 for the theoretical values of K_2.)

In the high-intensity region the term $rn(n+n_0)$ becomes important while $K_1\mathcal{S}$ can be neglected compared to $K_2\mathcal{S}^2$, thus only the second and last terms in Eq. (2) need to be considered in this case. The lifetime $[r(n+n_0)]^{-1}$ also becomes small compared to Δt and therefore the relation between $\sigma_{ex,max}$ and $\mathcal{S}_{max}$ is now described by the steady-state solution of Eq. (2):

$$\sigma_{ex,max} = e\mu (K_2/r)^{1/2} (1-R)\, \mathcal{S}_{max} . \quad (4)$$

Equation (4) fitted to the experimental curve in the high-intensity region yields $r = 6.9\times 10^{-9}$ cm^3/sec.

The value of r obtained from decay measurements is $r \approx 1.2\times 10^{-9}$ cm^3/sec.[6] This value is measured for $n \approx 10^{14}$ cm^{-3}. Since r is expected to increase for high values of n as explained in Ref. 6 and $n \gtrsim 10^{15}$ cm^{-3} in the high-intensity region at 2 °K, the values obtained for r are consistent.

As noted above, the results obtained with the 10.6-μm irradiation are quite different from the results obtained with $\lambda = 9.6$ μm. A photon with $\lambda = 10.6$ μm has an energy slightly less than one-half the bandgap energy in InSb at 2 °K. The two-photon transition is therefore forbidden at this temperature for $\lambda = 10.6$ μm. As Fig. 2 shows, this causes $\sigma_{ex,max}$ to increase as $\mathcal{S}_{max}^{1/2}$ in both the intermediate- and the high-intensity regions because the only generation is given by $K_1\mathcal{S}$ and the loss by $rn(n+n_0) \approx rn^2$. For the focused 10.6-μm laser beam the slope for high values of $\mathcal{S}_{max}$ is larger than $\frac{1}{2}$. The explanation is assumed to be that these high excitation intensities heat the sample sufficiently to reduce the bandgap energy below $2\hbar\omega_{10.6}$ and thereby make the two-photon excitation possible also for $\lambda = 10.6$ μm. A high-intensity region similar to the results for 9.6-μm irradiation is then obtained.

Equation (3) is also valid in the low-intensity region for $\lambda = 10.6$ μm. Curve fitting in this region yields $K_1 = 6.3\times 10^{10}$ $\text{erg}^{-1}\text{sec}^{-1}$.

b. At liquid-N_2 temperature. Figures 3 and 4 show $\sigma_{ex,max}$ as a function of $\mathcal{S}_{max}$ measured at 77 °K for two samples cut from different boules of n-type InSb. At this temperature the results obtained with 10.6- and 9.6-μm irradiation are similar and have the same general behavior as the results obtained at 2 °K with $\lambda = 9.6$ μm, except for the intermediate region. At 77 °K in this region the

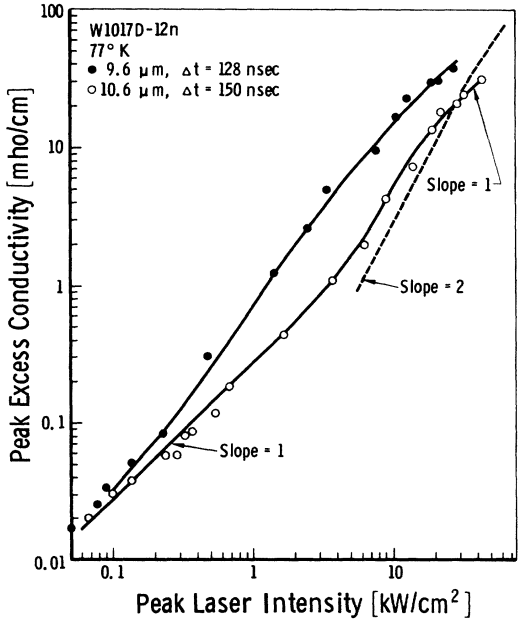

FIG. 3. Peak value of excess conductivity as a function of peak incident laser intensity (unfocused laser beam). The dashed line corresponds to data of Danishevskii *et al.* The carrier lifetime is $\tau = 730$ nsec.

slope in the log-log plots varies from a high value of 2 to a low value of less than 1.

Since $n/\tau \gg r n(n+n_0)$ at 77 °K, the term $r n(n+n_0)$ can be omitted from Eq. (2) at this temperature. Furthermore, for the two boules measured $\tau \gg \Delta t$, and the maximum value of σ_{ex} is obtained during the duration of the laser pulse, as is the case at 2 °K, thus the term n/τ can be neglected.

Equation (3) is valid for the low-intensity region and in most cases also for the intermediate-intensity region. Curve fitting in the low-intensity region yields the values for K_1 listed in Table II. The intermediate region is more complicated than at 2 °K because of an extra loss term described below. In the cases when this extra loss term does not disturb the lower part of the intermediate-intensity region, the curve fitting necessary to obtain K_2 is made easier by subtracting the straight line $\sigma'_{ex,max} = 1.06 e \mu \Delta t K_1 (1-R)\, g_{max}$ from the measured values of $\sigma_{ex,max}$. The resulting curve depends quadratically on g_{max}. K_2 is then obtained by fitting the expression $\sigma_{ex,max} - \sigma'_{ex,max} = 0.75 e \mu \Delta t K_2 (1-R)^2 (g_{max})^2$ to this curve. The resulting values of K_2 are typically 0.6 cm sec/erg^2 for 9.6-μm irradiation, and 0.05 cm sec/erg^2 for $\lambda = 10.6$ μm. (See Ref. 5 for the theoretical values.)

The high-intensity region is at the present time not well understood. It was first thought that this linear region is a consequence of a steady-state solution of Eq. (2), as is the case at 2 °K. However, the value of r at 77 °K is apparently so small

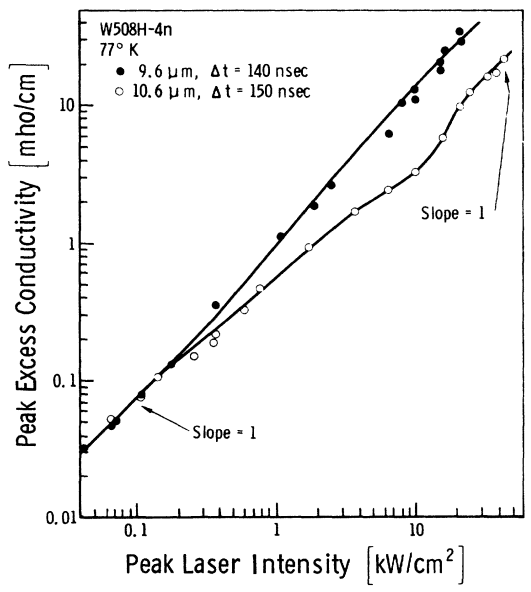

FIG. 4. Peak value of excess conductivity as a function of peak incident laser intensity (unfocused laser beam). The carrier lifetime is $\tau = 600$ nsec.

TABLE II. Linear excitation coefficient K_1 at 77 °K.

Sample no.	W1017D − 12n		W508H − 4n	
λ[μm]	10.6	9.6	10.6	9.6
K_1[10^9 erg^{-1} cm^{-1}]	2.5	4.0	7.0	7.4

that for the excess-carrier densities obtained in these experiments the last term is insignificant.[6] Reference 6 shows the insignificance of the last term both by a calculation of the value of r and by measurements of the decay of excess carriers. The decay is exponential after the laser pulse is cut off, even for the highest achievable values of n. This exponential decay proves that the term n/τ is larger than the term $r n(n+n_0)$ even for the high-intensity region.

The second term cannot account for the observed linearity. The second-order coefficient K_2 is expected to decrease with increasing n for high values of n [see Ref. 5, Eqs. (11) and (12)] but not sufficiently to explain the linear dependence between $\sigma_{ex,max}$ and g_{max}. In fact, we have shown[5] that for values of n as high as 10^{15} cm^{-3} the decrease in K_2 is negligible compared to the magnitude of K_2. The highest value of $\sigma_{ex,max}$ in Figs. 3 and 4 is ~ 50 Ω^{-1} cm^{-1} corresponding to $n \approx 5 \times 10^{14}$ cm^{-3}.

Since K_2 does not change appreciably and $r n^2 \ll n/\tau$, another loss term is needed in Eq. (2) to obtain $\sigma_{ex,max} \propto g_{max}$. This extra loss term should have the form bng and during irradiation it should be $\gg n/\tau$. Then the steady-state solution for high values of g becomes $n = (K_2/b)\, g$ and, therefore, $n_{max} = (K_2/b)\, g_{max}$. After the laser pulse is cut off, the term bng vanishes and the decay is determined by n/τ. A term of the form $\partial n/\partial t = -bng$ may be caused by stimulated transition from the conduction band into an empty trapping level.

To check whether or not the apparent additional loss term could be caused by the illumination of the contact regions, the conductivity of sample $W1017D - 8n$ was measured with and without shaded contacts, but no significant differences are observable. Surface effects are also an unlikely source for the unknown loss, since samples with thickness varying from ~ 0.3 to ~ 1 mm show essentially the same behavior. We therefore believe that the unidentified loss term is caused by a bulk effect, most likely by a trapping level, as mentioned above.

B. Absorption Caused by Transitions between Valence Bands

The smallness of the coefficient K_2 causes the two-photon absorption to be negligible (even though the absorption produces a dense plasma) for the laser intensities and sample thicknesses used in the present experiments. However, when laser intensities in excess of ~ 100 kW/cm^2 are used,

considerable absorption of the laser light is measured in samples of ~ 1-mm thickness. This absorption is caused by single-photon transitions from the light- to the heavy-hole band.[11]

For the excess-carrier densities we generate, this absorption is proportional to the number of holes. It is therefore commonly, although somewhat misleadingly, referred to as "free-hole absorption."

If z is chosen to be in the propagation direction of the laser beam,

$$\frac{\partial \mathcal{I}(z)}{\partial z} = -qn\,\mathcal{I}(z)\,, \tag{5}$$

where q is the free-hole-absorption cross section. Since this absorption is important only in the high-intensity region, we will restrict the following discussion to this region and assume a linear relation between n and $\mathcal{I}$ at every position in the sample as the data (Figs. 2–4) suggest are reasonable (steady-state solution),

$$n(z) = a\,\mathcal{I}(z)\,. \tag{6}$$

The coefficient a is obtained from the $\sigma_{ex,max}$-vs-$\mathcal{I}_{max}$ curves. Combining Eqs. (5) and (6) produces an absorption that depends nonlinearly on $\mathcal{I}$:

$$\frac{\partial \mathcal{I}(z)}{\partial z} = -qa\mathcal{I}^2(z)\,. \tag{7}$$

In Secs. III B a, III B b, and III B c three consequences of this absorption are shown. First the the direct attenuation of the laser beam, then its influence upon the average measured $\sigma_{ex,max}$, and, finally, shaping of the laser pulse.

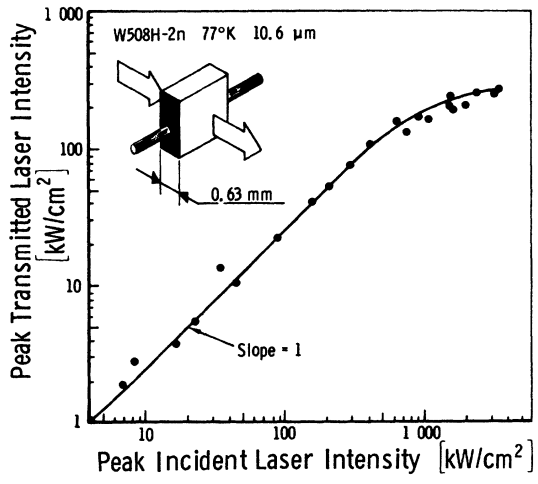

FIG. 5. Peak transmitted intensity as a function of incident laser intensity (focused beam). The insert shows the sample/beam geometry and a set of contacts used in the conductivity measurements. A 0.62-mm aperture is placed in front of the sample (not shown).

a. Absorption measurements. Figure 5 shows the results of absorption measurements at 77 °K on a sample from the same boule as the sample used to obtain the data given in Fig. 4. To maximize the laser intensity its beam was focused. A rather large pinhole, diam = 0.62 mm, is placed in front of the 1.0×1.0×0.63-mm sample. If we make the crude approximation that the illumination is uniform across this aperture and that a negligible number of carriers diffuses away from the excited region of the sample, we may use Eq. (7) to calculate the variation of $\mathcal{I}$ along z. Integration of Eq. (7) yields

$$\mathcal{I}(z) = \mathcal{I}(0)/[1+qaz\mathcal{I}(0)]\,. \tag{8}$$

As pointed out by Arsen'ev *et al.*,[12] Eq. (8) shows that for large values of $\mathcal{I}(0)$, $\mathcal{I}(z)$ reaches a saturated value, $\mathcal{I}(z)_{sat} = 1/qaz$. Taking the reflection from the far-end surface of the sample into consideration yields

$$\mathcal{I}_{tr,sat} = (1-R)/qad\,. \tag{9}$$

The quantity $\mathcal{I}_{tr,sat}$ is the maximum value of the laser intensity transmitted through the sample with thickness d.

Figure 5 shows that the measured value is $\mathcal{I}_{tr,sat} \approx 300$ kW/cm^2. This value together with $d = 0.063$ cm, $R = 0.36$,[13] and $a = 650$ sec/erg cm, substituted into Eq. (9), gives $q \approx 5\times10^{-15}$ cm^2. The coefficient a is obtained by using Eq. (6) and the experimental $\sigma_{ex,max}$-vs-$\mathcal{I}_{max}$ data in the high-intensity region, Fig. 4.

The value of q obtained this way is less than a factor 2 larger than the value obtained from linear absorption measurements by Kurnick and Powell.[11] This is a good agreement particularly considering our approximations.

For low intensities there is negligible absorption in the bulk of the material, and the only loss is caused by reflections. Taking multiple reflections into account and assuming no interference, the laser intensity is reduced by a factor, $(1-R)/(1+R)$, when it passes through the sample. The reflection coefficient of InSb is 0.36, thus $(1-R)/(1+R) = 0.47$. The experimental value obtained from the data of Fig. 5 is 0.25. This discrepancy is larger than we expected. Besides the possibility that the discrepancy may be caused by inaccuracy in the measurements, another possibility is scattering of the laser light in the bulk of the sample.

b. Effect on conductivity measurements. From Eqs. (6) and (8) and the relation $\sigma_{ex} = e\mu n$ we obtain $\sigma_{ex}(z)$. The average value of σ_{ex} is then found by integrating $\sigma_{ex}(z)$ along the thickness of the sample. The result is

$$\langle\sigma_{ex}\rangle_{av} = (e\mu/qd)\ln[1+qda\,\mathcal{I}(0)]\,. \tag{10}$$

For small values of $\mathcal{I}(0)$ the free-hole absorption

is negligible and Eq. (10) reduces to $\langle\sigma_{ex}\rangle_{av} = e\mu a \mathcal{I}(0)$. The average excess conductivity is proportional to $\mathcal{I}(0)$ for $\mathcal{I}(0) \ll 1/qad$. As $\mathcal{I}(0)$ increases the average σ_{ex} begins to saturate. When the excess conductivity is at its maximum, $\mathcal{I}(0)_{max} = (1-R)\mathcal{I}_{max}$. Note that $\mathcal{I}_{max}$ is the peak value of the laser irradiation impinging on the surface of the sample, while $\mathcal{I}(z)$ refers to the intensity inside the sample.

The data points in Fig. 6 show the experimental values of $\langle\sigma_{ex,max}\rangle_{av}$ as a function of $\mathcal{I}_{max}$. The three fitted curves are obtained from Eq. (10) using $\mathcal{I}(0)_{max} = (1-R)\mathcal{I}_{max}$, $a = 650$ sec/erg cm, and the value of q that gives the best fit to the data. The value obtained in this way for q is 1.5×10^{-14} cm^2, which is approximately one order of magnitude too large compared to the value measured in Sec. III B *a*.

This large discrepancy is in great contrast to the results obtained by Danishevskii *et al.*[2] They also observed the saturation in the average excess conductivity and reported that their results agreed with earlier data[11] for q with an accuracy of 1%. Another big difference between their results and ours is that they observed this saturation in the intermediate region rather than in the high-intensity region as in the present work. At this time we cannot explain the lack of agreement.

c. Shaping of laser pulse. The change of the laser pulse's time dependence after going through the sample is shown in Fig. 7 for both 2 °K and 77 °K. The shape of the incident beam is drawn with dashed lines. For low incident laser intensities the beam goes through the sample without shape change. For higher intensities, the transmitted beam initially follows closely the time dependence of the impinging beam up to a certain intensity, then drops sharply down to a low intensity

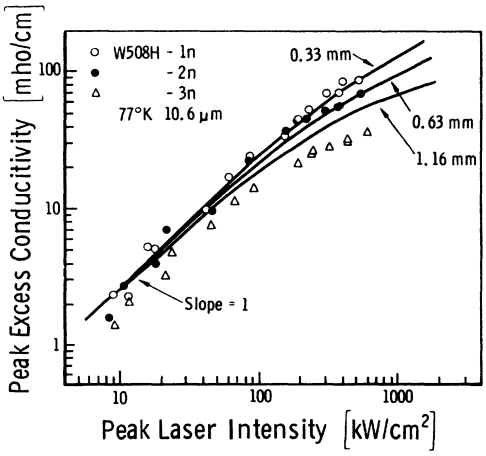

FIG. 6. Average $\sigma_{ex,max}$ as a function of peak incident laser intensity with thickness as a parameter (focused beam). See text for the meaning of the fitted curves.

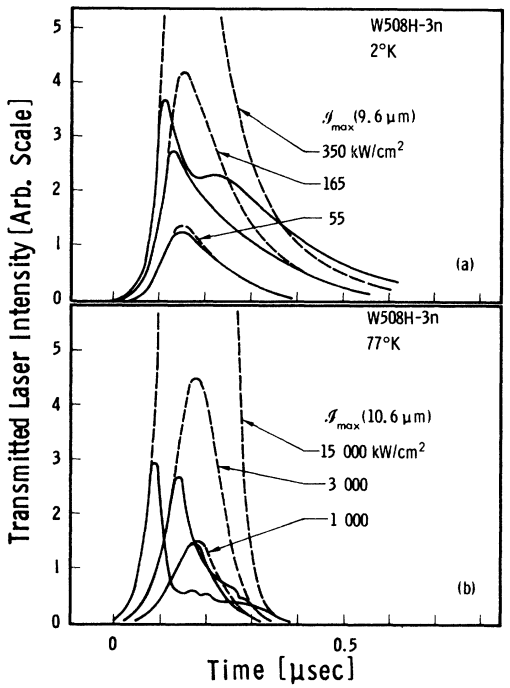

FIG. 7. Time dependence of transmitted laser intensity showing the pulse-shaping effect. The broken lines show the incident pulses and the solid lines show the transmitted pulses. Initially the incident and the transmitted pulses overlap. (a) $T = 2$ °K; (b) $T = 77$ °K.

and stays essentially at that level for the remaining duration of the incident laser pulse. The reason for this behavior is probably related to the fact that it takes a finite time to generate the electron-hole pairs. Therefore, at the beginning of the laser pulse there is no free-hole absorption. Later, when the excess carriers have been generated, the free-hole absorption reduces the transmitted light intensity.

C. Recombination Radiation

The number of photons, $N_{5.3}$, with wavelength 5.3 μm, generated per unit time in the sample, is give by the expression

$$\frac{\partial N_{5.3}}{\partial t} = rn(n+n_0). \tag{11}$$

In the density range in which we observe recombination radiation, $n \gg n_0$, so n_0 can be neglected in Eq. (11). If we also neglect reabsorption, as is shown to be a reasonable assumption in Ref. 6, the recombination intensity $\mathcal{I}_{5.3}$ at a given distance from the sample is proportional to $\partial N_{5.3}/\partial t$ and, therefore, $\mathcal{I}_{5.3} \propto n^2$.

Figure 8 shows the peak intensity of the recombination radiation measured by the Ge : Au detector behind the Dewar (Fig. 1) as a function of the

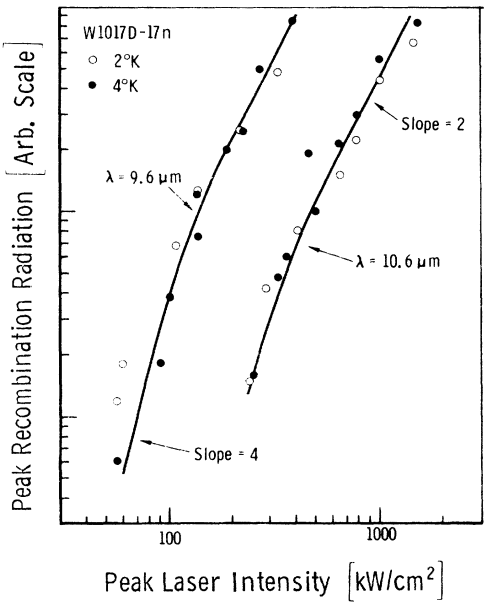

FIG. 8. Peak value of recombination-radiation intensity as a function of peak incident laser intensity for a sample of thickness 0.35 mm.

peak illumination intensity of the laser. The sample is immersed in liquid He, and the laser is focused. In the high-intensity region we see that $g_{5.3,\max} \propto (g_{\max})^2$. This is expected when 9.6-μm irradiation wavelength is used, since $n_{\max} \propto g_{\max}$ in this region.

The similarity in slope for the 9.6- and 10.6-μm data is unexpected, since Fig. 2 shows $n_{\max} \propto (g_{\max})^{1/2}$ for the longer wavelength. The explanation is assumed to be related to the heating of the sample, as discussed above in Sec. III A, so that $n_{\max} \propto g_{\max}$ in the high-intensity region and thus also $g_{5.3,\max} \propto (g_{\max})^2$.

As the excitation intensity is reduced the recombination-radiation curves (Fig. 8) become steeper and approach a slope of 4. This behavior is consistent with that in Fig. 2 for 9.6 μm since the intermediate-intensity region is characterized by $n_{\max} \propto (g_{\max})^2$. The upper-boundary value of the $g_{5.3,\max} \propto (g_{\max})^4$ region obtained from the conductivity data (Fig. 2) is ~ 10 kW/cm^2. This boundary between the high- and intermediate-intensity region is somewhat higher, ~ 80 kW/cm^2, according to the recombination data. For $\lambda = 10.6$ μm no comparison can be made since the two-photon excitation vanishes for this wavelength in Fig. 2.

The recombination radiation data shown in Fig. 8 are for a sample with a thickness of ~ 0.3 mm (Table I). For this sample the width of the recombination-radiation pulse is essentially the same as for the laser pulse and there is a very small time delay between the two pulses. If the thickness of the sample is increased, this behavior changes drastically. This is illustrated in Fig. 9 for 0.7-mm-thick sample where the time dependence of the recombination radiation is shown for various values of $g_{\max}$. For comparison, the laser pulse is shown in the upper part of the figure. For low values of $g_{\max}$ the width of the 5.3-μm radiation is essentially the same as the incident radiation; however, in contrast to the results with the 0.3-mm-thick sample, a significant delay between the laser pulse and the recombination radiation occurs. For the highest values of $g_{\max}$ the 5.3-μm pulse becomes considerably wider than the incident beam and the delay is lessened.

As yet we have no explanation of this behavior. The explanation is probably rather complex because several effects have to be considered. For relatively thick samples the assumption of uniformity along the z axis is invalid. Furthermore, the following effects may play significant roles; free-hole absorption, reabsorption or stimulated emission, heating of the sample, and internal reflections from the surface of the sample. Diffusion of excess carriers away from the illuminated region is expected to be mainly caused by emission and reabsorption of 5.3-μm photons and is, there-

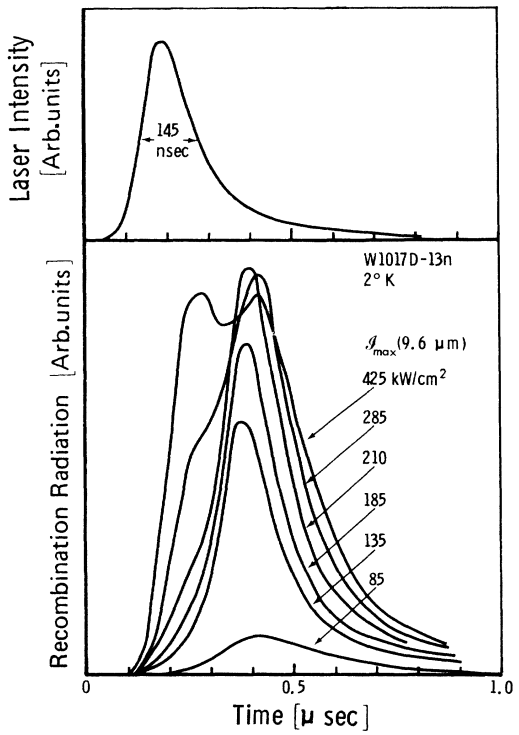

FIG. 9. Time dependence of recombination radiation for a sample of thickness 0.7 mm. The time dependence of the incident beam is shown above for comparison.

fore, already included in the above list.

Recombination radiation is also observed at 77 °K. The strength of the radiation at this temperature is much less than at liquid-He temperatures for a given g_{max}. This reduction in intensity is caused by increased reabsorption in the sample, since the absorption length at 77 °K is considerably smaller than the size of the sample; thus only the the photons generated in a surface layer of thickness approximately equal to the absorption length will escape from the sample. As shown in Fig. 10 the relationship $g_{5.3,max} \propto (g_{max})^2$ approximately holds at 77 °K. This agrees with the linear relation between $\sigma_{ex,max}$ and g_{max} obtained in the high-intensity region (Fig. 3).

IV. CONCLUSIONS

The measured peak excess conductivity as a function of peak irradiation intensity at 2 °K is now well understood. At 77 °K, however, only the results for the low- and intermediate-intensity region can be explained, while the high-region measurements do not fit our solution of the rate equation. The decay measurements show that the extra loss term needed to explain the high-intensity region is absent unless the laser radiation is present. This loss term is proportional to the product of plasma density and laser intensity. More work is necessary to confirm the presence of such a term and to discover its physical nature.

Measurements show that good uniformity of two-photon produced plasmas in samples up to 0.3-mm thickness is obtained for densities as high as 10^{15} cm^{-3}. This sample size is sufficiently large for several types of plasma experiments. The uniformity is much better than that obtainable by all known alternative means of electron-hole plasma generation. The density is an order of magnitude higher than achieved previously, except in plasma pinches which have essentially uncontrollable densities and suffer from several instabilities. Our plasmas are stable, since no applied fields are required in their generation.

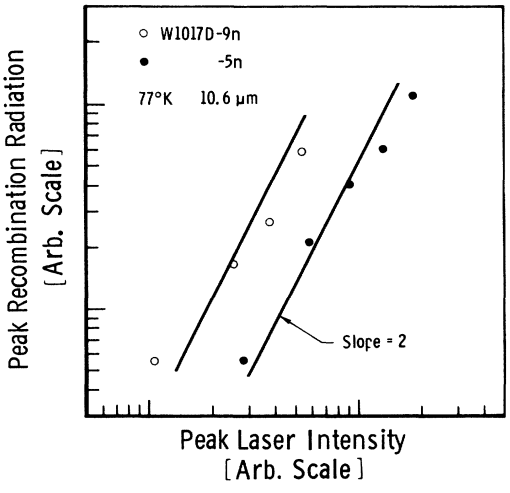

FIG. 10. Peak value of recombination-radiation intensity as a function of peak incident laser intensity.

Single-photon excitation of an electron from the light-hole band into the heavy-hole band (often called "free-hole absorption") is shown to be responsible for limiting both the maximum densities that may be achieved by this optical generation technique and also the thickness of samples possessing highly uniform plasmas.

A novel effect is reported, namely, a change in the temporal shape of a high-intensity laser beam during passage through the sample. This pulse-shaping effect is caused by free-hole absorption which depends nonlinearly on the laser intensity. Meaningful comparison between the measured results and the theory requires further work. The rate equation and the expression for the free-hole absorption should be solved simultaneously using a computer.

ACKNOWLEDGMENTS

The authors wish to thank Dr. D. B. Chang for many stimulating discussions, J. O. Page for constructing most of the experimental apparatus, and R. M. Lantz for his expert technical assistance.

APPENDIX A: CONTACTS

The reason for using exclusively n-type InSb in the present work is that it is possible to make more nearly Ohmic contacts on this material than on p-InSb. Contacts are made by alloying to the surface of the semiconductor either indium containing 1-wt.% tellurium or indium containing 20-wt.% cadmium to obtain n- or p-doped contact regions, respectively.

For the present study Ohmic contact with low recombination velocity at the contact surface are needed. A simple model that describes the influence the contacts have on the effective decay of the excess-carrier density follows. Figure 11 shows a sample. It consists of the bulk of the semiconductor (designated by B) and two contacts which consist of a thin region (thickness δ, exaggerated in Fig. 11) with high doping density connected to an ideal contact, i.e., a contact possessing infinite surface recombination velocity at $x = \pm(\frac{1}{2}l + \delta)$. Consider in the following a p^+pp^+ device where the p^+ region and the p region (which is B) have a doping concentration N_+ and N_B, respectively. Charge neutrality is required throughout the device (except for the junction space-charge region). The excess-carrier density in the two regions will be designated by n_+ and n_B. Because of symmetry only $x > 0$ need be considered. The fol-

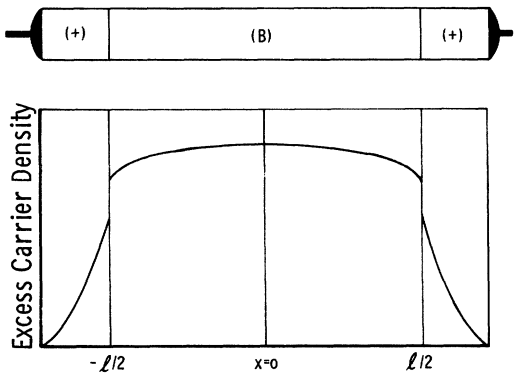

FIG. 11. Diagram showing the diffusion loss of excess carriers from the bulk to the contact regions.

lowing boundary conditions are used:

$$n_+(\tfrac{1}{2}l+\delta)=0, \tag{A1}$$

$$\left(\frac{\partial n_B}{\partial x}\right)_{x=0}=0, \tag{A2}$$

$$D_B\left(\frac{\partial n_B}{\partial x}\right)_{x=l/2}=D_+\left(\frac{\partial n_+}{\partial x}\right)_{x=l/2}, \tag{A3}$$

and[14]

$$n_+(\tfrac{1}{2}l)=n_B(\tfrac{1}{2}l)[n_B(\tfrac{1}{2}l)+N_B]/N_+ . \tag{A4}$$

Here D_B and D_+ are ambipolar diffusion constants in the bulk and in the heavily doped region, respectively.

Solution of the diffusion equation

$$\frac{\partial n_i}{\partial t}=D_i\frac{\partial^2 n_i}{\partial x^2}-\frac{n_i}{\tau_i}, \tag{A5}$$

where $i=B, +$, is greatly simplified if we use the experimental fact that σ_{ex} and thus also n_B decay exponentially at 77 °K, and assume $\partial n_i/\partial t=-n_i/\tau$. Here τ is the measured decay time for σ_{ex}. Thus the diffusion equation is reduced to

$$\frac{\partial^2 n_i}{\partial x^2}=\frac{n_i}{L_i^2}, \tag{A6}$$

where

$$1/L_i^2=(1/\tau_i-1/\tau)/D_i . \tag{A7}$$

If Eqs. (A1)–(A7) are combined, the following relation between L_B and the excess conductivity in the center of the sample, $n_B(0)\equiv n$, is obtained:

$$-\frac{L_+}{|L_B|}\tan\left(\frac{l}{2|L_B|}\right)\tanh\left(\frac{\delta}{L_+}\right)=\frac{D_+ n}{D_B N_+}\left[\cos\left(\frac{L}{2|L_B|}\right)+\frac{N_B}{n}\right]. \tag{A8}$$

If $\tau_+=10^{-9}$ sec ($\ll\tau$) and $D_+\approx 4000$ cm^2/sec are used for the highly doped p^+ region, $L_+=20$ μm is obtained. This value of L_+ is larger than the thickness of the p^+ region, δ, and therefore $\tanh(\delta/L_+)\approx\delta/L_+$. Assuming $|L_B|>l$, as is justified since $\tau\approx\tau_B$, then $\tan(l/2|L_B|)\approx l/2|L_B|$ and $\cos(\frac{1}{2}l|L_B|)\approx 1$. These approximations together with $n\gg N_B$ used in Eq. (18) give

$$1/L_B^2\approx -2nD_+/(N_+D_B l\delta)$$

or

$$1/\tau\approx 1/\tau_B+2nD_+/(N_+l\delta) . \tag{A9}$$

The expression for $1/L_B^2$ shows that the validity of the approximation $|L_B|>l$ depends on the value of the excess-carrier density.

The same expression for τ given by Eq. (A9) can be obtained for a n^+pn^+ sample. The only difference is the value of D_+, which for a n^+ region is equal to the diffusion constant for holes, $D_p\approx 50$ cm^2/sec. The second term on the right-hand side of Eq. (A9), which represents the loss through the contacts, is therefore larger by a factor $D_n/D_p\approx 80$ for p^+ contacts compared to n^+ contacts. This shows why p^+ contacts are more lossy than n^+ contacts.

This difference in the types of contacts is readily observed. Figure 12 shows the decay of the excess conductivity for two p-type samples with different contacts. The sample with p^+ contacts has a faster decay rate than the one with n^+ contacts, except at very low excess conductivity. The data of Fig. 12 agree well with the description given above. The n^+pn^+ sample, however, has the disadvantage of a considerable voltage drop across the back-biased junction at low excess conductivity. This effect is clearly shown by the data because the excess conductivity of n^+pn^+ samples approach zero rapidly in contrast to the more asymptotic approach to

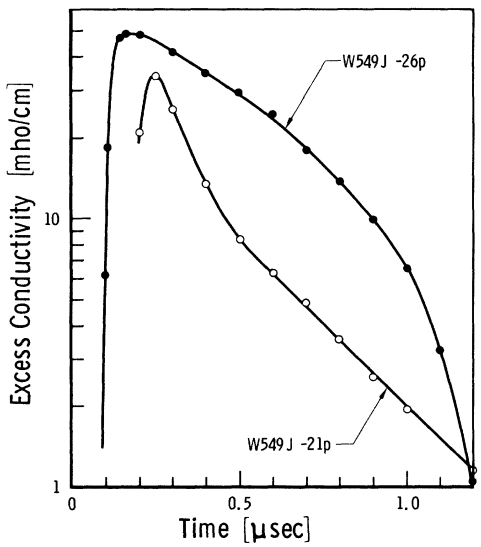

FIG. 12. Decay of excess conductivities for n^+pn^+ ($W549J-21p$) and p^+pp^+ ($W549J-26p$) samples.

zero of p^+pp^+ samples (Fig. 12).

By using n-type material with n^+ contacts this disadvantage is completely avoided. Indeed, such a sample possesses all the desirable properties: small loss of carriers in the high-density region and good Ohmic behavior (no back-biased junction) in the low-density region.

APPENDIX B: LOW-TEMPERATURE CONDUCTIVITY MEASUREMENTS

At liquid-He temperatures the electron mobility depends on both the applied electric field E and the excess-carrier density n. Without knowing these dependencies in detail the excess-carrier density cannot be determined accurately from conductivity measurements.

In an effort to estimate the accuracy of our experimentally deduced values of n, the current through the sample for two applied voltages is measured with the excess conductivity obtained by irradiation as a parameter. The results are plotted in Fig. 13 together with our measured current-voltage characteristic for $\sigma_{ex} = 0$.

The nonlinear current-voltage relation for samples with no excess carriers is described by Putley[9] and attributed to the hot electron effect. According to Putley the conductivity is proportional to $1+\beta E^2$ for $E \leq 0.1$ V/cm, where β is a constant that depends on the temperature. Then, for higher electric field the conductivity increases more steeply until E is ~ 0.2 V/cm; at higher E the relation between current and electric field is substantially linear. This description fits our measured current-voltage relation for $\sigma_{ex} = 0$ (Fig. 13). Our measurements indicate further that for increasing excess conductivity the nonlinear current-voltage relation disappears; for $\sigma_{ex} \geq 2.7$ mho/cm the relation is evidently linear.

Our findings thus indicate that the conductivity, σ, is independent of E as long as $\sigma_{ex} \geq 2.7$ mho/cm. For smaller values of σ_{ex}, the value of σ is only meaningful when the value of E is also given.

We apply routinely $E = 0.4$ V/cm in order to measure conductivity and thus deduce n. As σ_{ex} increases because of exposure to radiation, E decreases. As an example E, in sample *W1017D – 12n*, drops to 0.28 V/cm for $\sigma_{ex} = 2.7$ mho/cm, the boundary value for linear current-voltage characteristics. The E observed at the boundary differs somewhat from sample to sample because σ_0 and the cross section vary. For none of the measured samples, however, is this field less than 0.2 V/cm. The difference between the measured value of σ_{ex} and the value for $E = 0.4$ V/cm is thus less than the difference between the equilibrium conductivity for $E = 0.2$ and 0.4 V/cm, which is ~ 40%. A more reasonable estimate of the error is 20% because there is a gradual change from the linear current-voltage relation to the nonlinear relation for $\sigma_{ex} = 0$ and we have chosen the worst case for the error calculation.

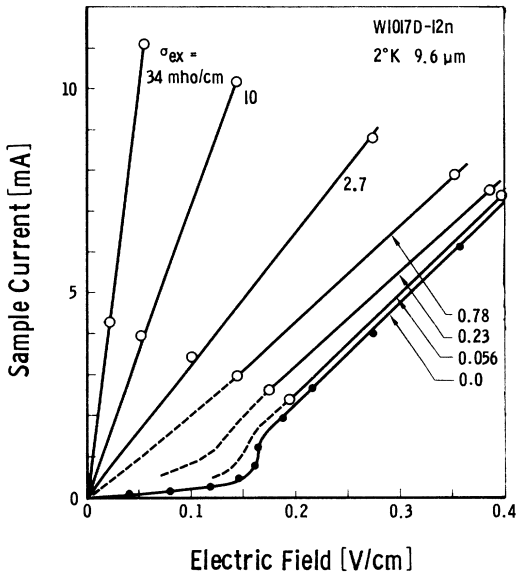

FIG. 13. Current as a function of applied electric field. The parameter is the excess conductivity, σ_{ex}, given in mho/cm.

The value of the electron mobility at liquid-He temperatures used in the present work, is taken from Ref. 10, $\mu = 10^5$ cm^2/V sec. It was obtained from measurements on two n-type samples with donor density $\approx 10^{16}$ cm^{-3}. At this high electron concentration it is likely that μ is fairly independent of E. Martin and Mead[15] measured in 1970 the electron mobility for a n-type-InSb sample with an equilibrium carrier density of 10^{14} cm^{-3}. They obtained $\mu \approx 1.5 \times 10^5$ cm^2/V sec for $E = 0.4$ V/cm and $T \leq 12$ °K.

From the above considerations we conclude that the accuracy we can expect for our measurements of n is ~ 50%. A considerably better accuracy could be obtained by measuring the mobility as a function of both n and E at these low temperatures if the greater accuracy were worth the effort.

*Research partially supported by the Air Force Office of Scientific Research under Contract No. F44620-71-C-0055, and by the National Science Foundation under Grant No. GK 283884.

†Work done in partial fulfillment of the requirements for the Ph.D. degree at the University of Washington.

‡Present address: Norwegian Defence Research Establishment, Kjeller, Norway.

§Present address: United States Department of Commerce, Washington, D. C. 20230.

[1]A. F. Gibson, M. J. Kent, and M. F. Kimmitt, Br. J. Appl. Phys. (J. Phys. D.) 1, 149 (1968).

[2]A. M. Danishevskii, A. A. Patrin, S. M. Ryvkin, and I. D. Yaroshetskii, Zh. Eksp. Teor. Fiz. **56**, 1457 (1969) [Sov. Phys.-JETP **29**, 781 (1969)].
[3]R. E. Slusher, W. Giriat, and S. R. J. Brueck, Phys. Rev. **183**, 758 (1969).
[4]S. Hongo, S. Panyakeow, J. Shirafuji, and Y. Inuishi, Jap. J. Appl. Phys. **10**, 717 (1971).
[5]H. J. Fossum and D. B. Chang, second preceeding paper, Phys. Rev. B 8, 2842 (1973).
[6]H. J. Fossum and B. Ancker-Johnson, preceeding paper, Phys. Rev. B 8, 2850 (1973).
[7]B. Ancker-Johnson, H. J. Fossum, and W. S. Chen, Boeing document No. D180-15000-1, May, 1972 (unpublished).
[8]This was also used by Slusher *et al.*, see Ref. 3.
[9]E. H. Putley, *Semiconductors and Semimetals*, edited by R. K. Willardson and A. C. Beer (Academic, New York, 1966), Vol. 1, pp. 289–313; see especially pp. 299–301.
[10]C. Hilsum and A. C. Rose-Innes, *Semiconducting III-V Compounds* (Pergamon, New York, 1961), p. 126.
[11]S. W. Kurnick and J. M. Powell, Phys. Rev. **116**, 597 (1959).
[12]V. V. Arsen'ev, V. S. Dneprovskii, D. N. Klyshko, and A. N. Penin, Zh. Eksp. Teor. Fiz. **56**, 760 (1969) [Sov. Phys.-JETP **29**, 413 (1969)].
[13]B. O. Seraphin and H. E. Bennett, in Ref. 9, Vol. 3, pp. 499–543; see especially p. 542.
[14]D. L. Scharfetter, R. W. Lade, and A. G. Jordan, IEEE Trans. Electron Devices **ED10**, 35 (1963).
[15]J. P. Martin and J. B. Mead, Appl. Phys. Lett. **17**, 320 (1970).